JEM Journal of Experimental Medicine

BRIEF DEFINITIVE REPORT

IL-7–dependent maintenance of ILC3s is required for normal entry of lymphocytes into lymph nodes

Jie Yang[1], Ferry Cornelissen[3], Natalie Papazian[3], Rogier M. Reijmers[3], Miriam Llorian[4], Tom Cupedo[3], Mark Coles[2*], and Benedict Seddon[1*]

IL-7 is essential for the development and homeostasis of T and B lymphocytes and is critical for neonatal lymph node organogenesis because *Il7*$^{-/-}$ mice lack normal lymph nodes. Whether IL-7 is a continued requirement for normal lymph node structure and function is unknown. To address this, we ablated IL-7 function in normal adult hosts. Either inducible *Il7* gene deletion or IL-7R blockade in adults resulted in a rapid loss of lymph node cellularity and a corresponding defect in lymphocyte entry into lymph nodes. Although stromal and dendritic cell components of lymph nodes were present in normal numbers and representation, innate lymphoid cell (ILC) subpopulations were substantially decreased after IL-7 ablation. Testing lymphocyte homing in bone marrow chimeras reconstituted with *Rorc*$^{-/-}$ bone marrow confirmed that ILC3s in lymph nodes are required for normal lymphocyte homing. Collectively, our data suggest that maintenance of intact lymph nodes relies on IL-7–dependent maintenance of ILC3 cells.

Introduction

The cytokine IL-7 is critical for the development of the lymphoid system. It has an obligate role in supporting development of B cell progenitors in the bone marrow (von Freeden-Jeffry et al., 1995). Similarly, in the thymus, survival and differentiation of early αβ T lineage precursors are dependent on IL-7 as is the specification of the γδ T cells (von Freeden-Jeffry et al., 1995; Ye et al., 2001). In addition to supporting lymphocyte development, IL-7 also plays a key role in promoting the normal development of lymph nodes in neonatal mice (Coles et al., 2006). Organogenesis of lymph nodes is orchestrated by interactions between stromal and endothelial lymphoid tissue organizer (LTo) cells (Cupedo et al., 2004; Onder et al., 2013) and hematopoietic lymphoid tissue inducer (LTi) cells, which are now identified as a RORγt-expressing member of the innate lymphoid cell family (ILC3; Sun et al., 2000; Eberl et al., 2004). Although maturation of LTo cells is dependent on lymphotoxin (LT) signaling, ILC3s in developing lymph nodes rely on IL-7 for development and proliferation, and IL-7–deficient mice have severely reduced numbers of all ILC3 populations (Satoh-Takayama et al., 2010) and consequently exhibit defective lymph node development (Coles et al., 2006).

In fully mature lymph nodes, these cellular components persist and continue to play important functions in lymph node homeostasis and immune function. Stromal cell components, such as fibroblastic reticular cells (FRCs), secrete T cell trophic chemokines CCL19 and 21 and therefore play critical roles in driving cellular localization within nodes (von Andrian and Mempel, 2003). There is also a continued requirement for LT signaling. In mature nodes, LT produced by dendritic cells (DCs) regulates functionality of high endothelial venule (HEVs; Moussion and Girard, 2011; Wendland et al., 2011), promoting expression of L-selectin ligands and therefore migration of lymphocytes into lymph nodes (Browning et al., 2005). IL-7 is produced within lymph nodes by both FRCs (Link et al., 2007) and lymphatic endothelial cells (LECs; Onder et al., 2012) and is critical for long-term survival of all major αβ T cell subsets (Schluns et al., 2000; Seddon and Zamoyska, 2002). Although it is clear IL-7 signaling plays a critical role in developing fully mature lymph node structures, it is unknown whether IL-7 continues to have a function in maintaining normal lymph node integrity beyond its influence on mature T cell survival.

In the present study, we investigated whether continued IL-7 expression was required for the maintenance of fully developed, adult lymph nodes. We tested this both by ablating IL-7 expression genetically and inhibiting IL-7 signaling by receptor blockade. Our study reveals a critical role for IL-7 in the maintenance of lymph node size in adults and as a requirement for T and B cell entry and provides evidence of a mechanism dependent not on LT signaling but rather on maintenance of ILC3 populations.

[1]Institute of Immunity and Transplantation, Division of Infection and Immunity, University College London, Royal Free Hospital, London, England, UK; [2]Kennedy Institute of Rheumatology, University of Oxford, Oxford, England, UK; [3]Department of Hematology, Erasmus University Medical Center, Rotterdam, Netherlands; [4]The Francis Crick Institute, Kings Cross, London, England, UK.

*M. Coles and B. Seddon contributed equally to this paper; Correspondence to Benedict Seddon: benedict.seddon@ucl.ac.uk; Mark Coles: mark.coles@york.ac.uk.

Results and discussion

Generation of mice with conditional *Il7* loci

To facilitate the study of IL-7 in adult mice, we generated a strain with a modified *Il7* allele that permits conditional gene ablation by using the Cre-Lox system (see Materials and methods). In brief, embryonic stem (ES) cells with the targeted $Il7^{tm1a(EUCOMM)Wtsi}$ locus were obtained from the European Conditional Mouse Mutagenesis Program consortium. Targeting resulted in FRT-site–flanked LacZ and neomycin resistance (*Neo*) cassettes upstream of exon 3 and LoxP recombination sites both flanking the neomycin cassette and downstream of exon 4 (Fig. S1 A). To test the functionality of the modified allele, $Il7^{tm1a(EUCOMM)Wtsi}$ mice were bred with PC3-Cre mice to induce germline deletion of the LoxP-flanked *Neo* cassette and exons 3 and 4 of the *Il7* gene but leaving LacZ gene expression intact and under control of endogenous *Il7* regulatory elements ($Il7^{LacZKO}$ allele; Fig. S1 A). LacZ and *Neo* cassettes were removed by breeding $Il7^{tm1a(EUCOMM)Wtsi}$ mice with actin-FlpE recombinase mice, which resulted in offspring in which exons 3 and 4 of *Il7* were flanked by LoxP sites ($Il7^{flox}$ allele; Fig. S1 A). Analysis of lymphoid compartments of mice homozygous for the $Il7^{LacZKO}$ allele revealed a phenotype consistent with existing *Il7* knockouts (von Freeden-Jeffry et al., 1995). Mice were lymphopenic, with reduced numbers of peripheral T and B cells in the lymph nodes and spleen (Fig. S1, B and C). Thymi were also small and exhibited an expected developmental block at the DN2 stage (Fig. S1 D). Together, these data confirmed the successful generation of a conditional *Il7* allele.

Conditional deletion of *Il7* gene in adult mice results in loss of T cell numbers and reduced lymph node sizes

To permit ablation of *Il7* gene expression in adults, $Il7^{flox}$ strain was bred with $Rosa26^{CreERT2}$ ($R26^{CreERT}$) mice, which ubiquitously express a tamoxifen hormone–inducible Cre. Tamoxifen was administered daily for 5 d to either $Il7^{flox/LacZKO}$ $R26^{CreERT}$ mice or Cre –ve littermates as control. *Il7* mRNA levels were measured in RNA extracted from whole-organ homogenates of the lymph nodes and spleen 3 wk after the first tamoxifen administration. This revealed a substantial reduction in the abundance of *Il7* mRNA in both the lymph node and spleen of $Il7^{flox/LacZKO}$ $R26^{CreERT}$ mice (Fig. 1 A). Basal levels of *Il7* mRNA were far higher in lymph nodes than in the spleen, consistent with studies of IL-7 reporter mouse strains (Kim et al., 2011).

In the absence of IL-7 signaling, T cells have a half-life of approximately 4 wk (Seddon and Zamoyska, 2002; Buentke et al., 2006). Consistent with this, after IL-7 gene deletion, analysis of total numbers of naive CD4 and CD8 T cells revealed more than a twofold reduction 4 wk after tamoxifen treatment (Fig. 1 B). However, analysis of different lymphoid subcompartments revealed an unequal distribution of naive cells. Unexpectedly, we observed a far greater and more rapid reduction of naive T cells in the lymph nodes than in the spleen by 2 wk (Fig. 1 B). It also appeared that total cellularity of lymph nodes was already far smaller at 2 wk than could be accounted for simply by the reduction in total T cell numbers (Fig. 1 C).

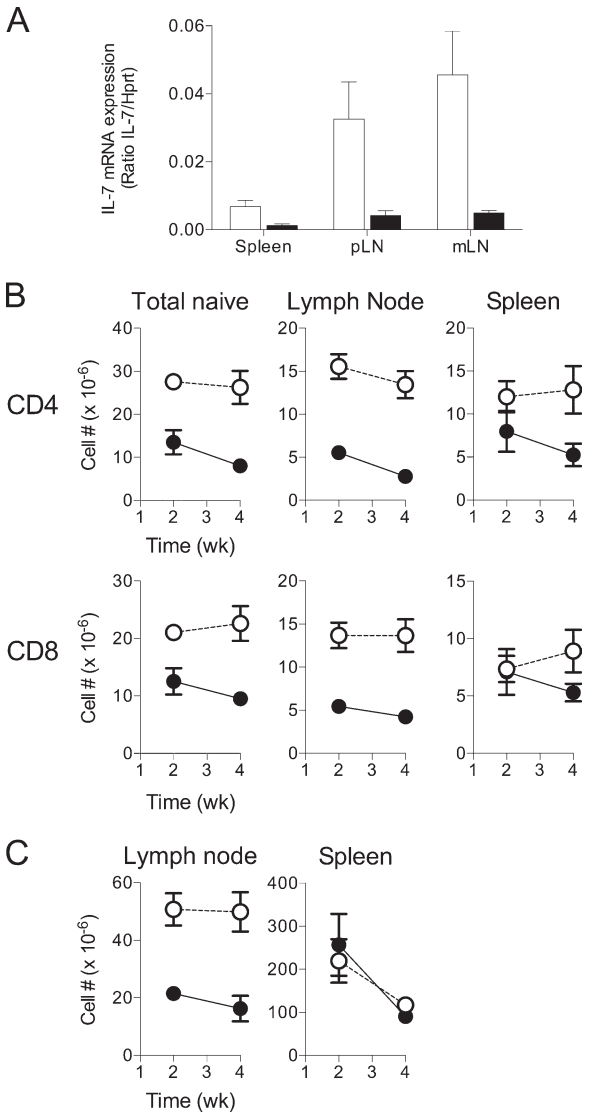

Figure 1. **Loss of naive T cells and lymph node size after ablation of IL-7 expression. (A)** Groups of $Il7^{fx/KO}$ $R26^{CreERT2}$ mice (n = 3, closed bars) were treated with tamoxifen for 5 d, and CreERT –ve littermates (n = 3, open bars) were also treated as controls. 3 wk later, total mRNA was isolated from whole-organ homogenates of mesenteric, peripheral lymph nodes and spleen, and *Il7* gene expression determined by real-time PCR. mRNA levels were normalized against *Hprt*. Bar charts show the relative abundance of *Il7* mRNA from different organs of the indicated donor mice. **(B)** Cohorts of $Il7^{fx/KO}$ $R26^{CreERT2}$ mice and CreERT –ve littermate controls were treated with tamoxifen for 5 d. Lymph nodes and the spleen were taken from groups of mice (n = 3 per group) 2 and 4 wk after treatment and analyzed by FACS. Graphs show total numbers of TCR^{hi} $CD44^{lo}$ $CD25^{-}$ naive CD4 and TCR^{hi} $CD44^{lo}$ naive CD8 T cells recovered from the indicated organs from $Il7^{fx/KO}$ $R26^{CreERT2}$ mice (closed symbols) vs. CreERT –ve littermate controls (open symbols). **(C)** Plots show total cell numbers recovered from the lymph nodes and spleen of the mice described in B. Data are representative of three or more independent experiments. Error bars show SEM.

T and B cell entry into lymph nodes is impaired after IL-7 deletion

The uneven distribution of naive T cells between the lymph nodes and the spleen suggested that the rapid reduction in lymph node size after ablation of IL-7 expression was not simply a consequence of changes to mature T and B cell compartment sizes.

It might instead reflect specific changes in lymph node homeostasis, such as lymphocyte entry via HEVs that are not present in spleen. To test this, we assessed the capacity of T cells from normal donors to home to lymph nodes of IL-7–deficient hosts in short-term migration experiments. Because donor cells were from unmanipulated mice, we could exclude any potential compounding effects of IL-7 deprivation on host T cell function. Total lymphocytes from CD45.1 donors were injected into $R26^{CreERT+}$ and $R26^{CreERT-}$ $Il7^{flox/LacZKO}$ hosts, 2–3 wk after their treatment with tamoxifen. Abundance of donor cells in the blood, spleen, and lymph nodes was assessed 1 h later. Frequencies of donor lymphocytes in the blood of different host mice was similar (Fig. 2 A), although there was a nonsignificant trend to greater numbers of donor cells in the spleen of $R26^{CreERT+}$ $Il7^{flox/LacZKO}$ hosts (Fig. 2 B). In contrast, both donor T and B cells were greatly reduced in numbers in lymph nodes from $R26^{CreERT+}$ $Il7^{flox/LacZKO}$ hosts compared with littermate $R26^{CreERT-}$ $Il7^{flox/LacZKO}$ hosts (Fig. 2 C). These data revealed defective entry of lymphocytes into lymph nodes of hosts lacking IL-7 expression.

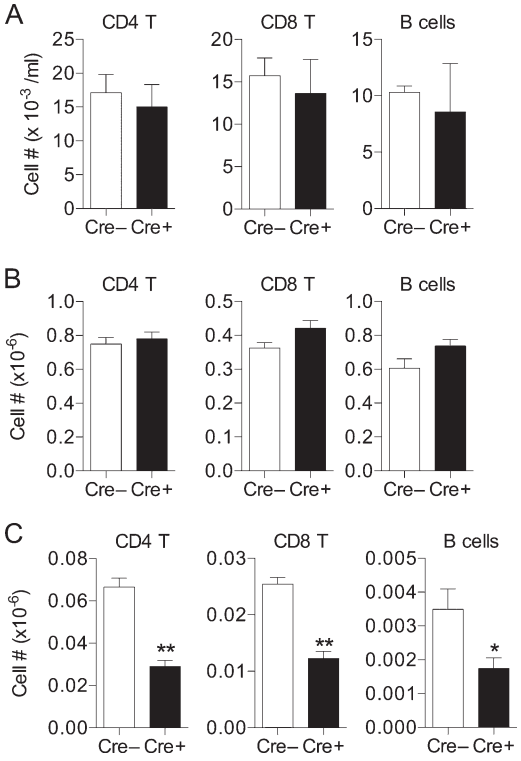

Figure 2. **Short-term homing of T and B cells to lymph nodes is impaired after IL-7 gene ablation.** $Il7^{fx/KO}$ $R26^{CreERT2}$ mice and CreERT –ve littermate controls (n = 6 per group) were treated with tamoxifen for 5 d. 2–3 wk later, hosts were injected i.v. with 10^7 total lymph node cells from congenic CD45.1 donors. 1 h later, mice were culled, and blood samples, lymph node cells, and splenocytes were analyzed by FACS. **(A–C)** Bar charts show the numbers of donor CD45.1+ CD4, CD8, and B lymphocytes in the blood (A), spleen (B), and lymph nodes (C) of $R26^{CreERT2}$ –ve (Cre–) and $R26^{CreERT2}$ +ve (Cre+) $Il7^{fx/KO}$ hosts at 1 h after transfer. Data are representative of three independent experiments. *, P < 0.05; **, P < 0.01. Error bars show SEM.

Normal stromal and DCs but reduced ILCs in the absence of IL-7

To investigate the mechanism by which IL-7 was regulating lymph node size, we asked whether key components of lymph node structure and function were affected by loss of IL-7 expression. FRCs and LECs are important structural components of lymph nodes and are also sources of IL-7 synthesis (Link et al., 2007; Onder et al., 2012), whereas blood endothelial cells (BECs) include HEVs that are key points of entry to lymph nodes. We therefore analyzed the phenotype and composition of stromal cell subsets after IL-7 deletion. We used expression of gp38 and CD31 by CD45$^-$ cells to identify gp38$^+$CD31$^-$ FRC and gp38$^+$CD31$^+$ LECs, as well as gp38$^-$CD31$^+$ BECs (Fig. 3 A). Importantly, despite the substantial reduction in lymph node size after IL-7 ablation, both numbers and representation of these stromal cell types were unaffected after the loss of IL-7 (Fig. 3 A). Entry of lymphocytes into lymph nodes via HEVs depends on lymphocyte adherence mediated by L-selectin and integrin binding and is stimulated by chemokines. Analyzing blood endothelia for expression of L-selectin and integrin ligands, PNAd and ICAM-1, respectively, did not reveal any defects after IL-7 ablation (Fig. 3 B). Histological analysis of PNAd and CD31 revealed normal HEV structures in lymph nodes after IL-7 ablation (Fig. 3 C). A more global analysis of gene expression within lymph nodes did not reveal any differences in expression of PNAd scaffolds and glycan synthetic enzymes required for appropriate glycosylation of scaffolds nor alterations in chemokine or LT expression (Fig. 3 D). DCs have also been implicated in regulating lymph node size both at steady state (Moussion and Girard, 2011; Wendland et al., 2011) and during immune responses (Acton et al., 2014). However, quantification of resident, migratory, and plasmacytoid DC populations revealed no detectable changes in numbers or composition after IL-7 deletion in either the lymph nodes or spleen (Fig. 3 E).

Finally, we analyzed the ILC composition of lymph nodes. ILC3 are critical for initial development and maturation of lymph node anlagen during embryogenesis and neonatal lymphoid colonization. Although their role in maintaining integrity and function of mature lymph nodes has not previously been assessed, it was possible they may continue to play a function after lymph nodes are fully developed. We therefore asked whether IL-7 ablation affected ILC numbers and/or representation in lymph nodes. In contrast to stromal and DC components, we did indeed observe substantial reductions in numbers of both ILC2 and ILC3 subsets in the lymph nodes and spleen after gene deletion (Fig. 3 F).

IL-7R blockade in T cell–deficient mice reduces ILC numbers and impairs lymphocyte entry into lymph nodes

Our results suggested that IL-7 is required for normal entry of lymphocytes into lymph nodes. To test whether this function of IL-7 was independent of its role in T and B lymphocyte homeostasis, we tested the effects of IL-7 blockade on lymphocyte entry into lymph nodes in T cell–deficient $Zap70^{-/-}$ hosts and $Rag1^{-/-}$ hosts that lack both T and B cells. We blocked IL-7 activity using the anti–IL-7R mAb A7R34 that inhibits binding of cytokine to the IL-7Rα chain (Sudo et al., 1993). Groups of $Zap70^{-/-}$ and $Rag1^{-/-}$ hosts were treated with anti-IL-7R for 2 wk. Controls were injected with either PBS or isotype control antibody. Analyzing ex vivo binding of A7R34 confirmed blockade of >90% of IL-7R on ILCs in lymph nodes (Fig. 4 A). Mice treated with anti–IL-7R exhibited a reduction in lymph node size but not spleen size (Fig. 4 B), as observed after IL-7 gene deletion. We then assessed

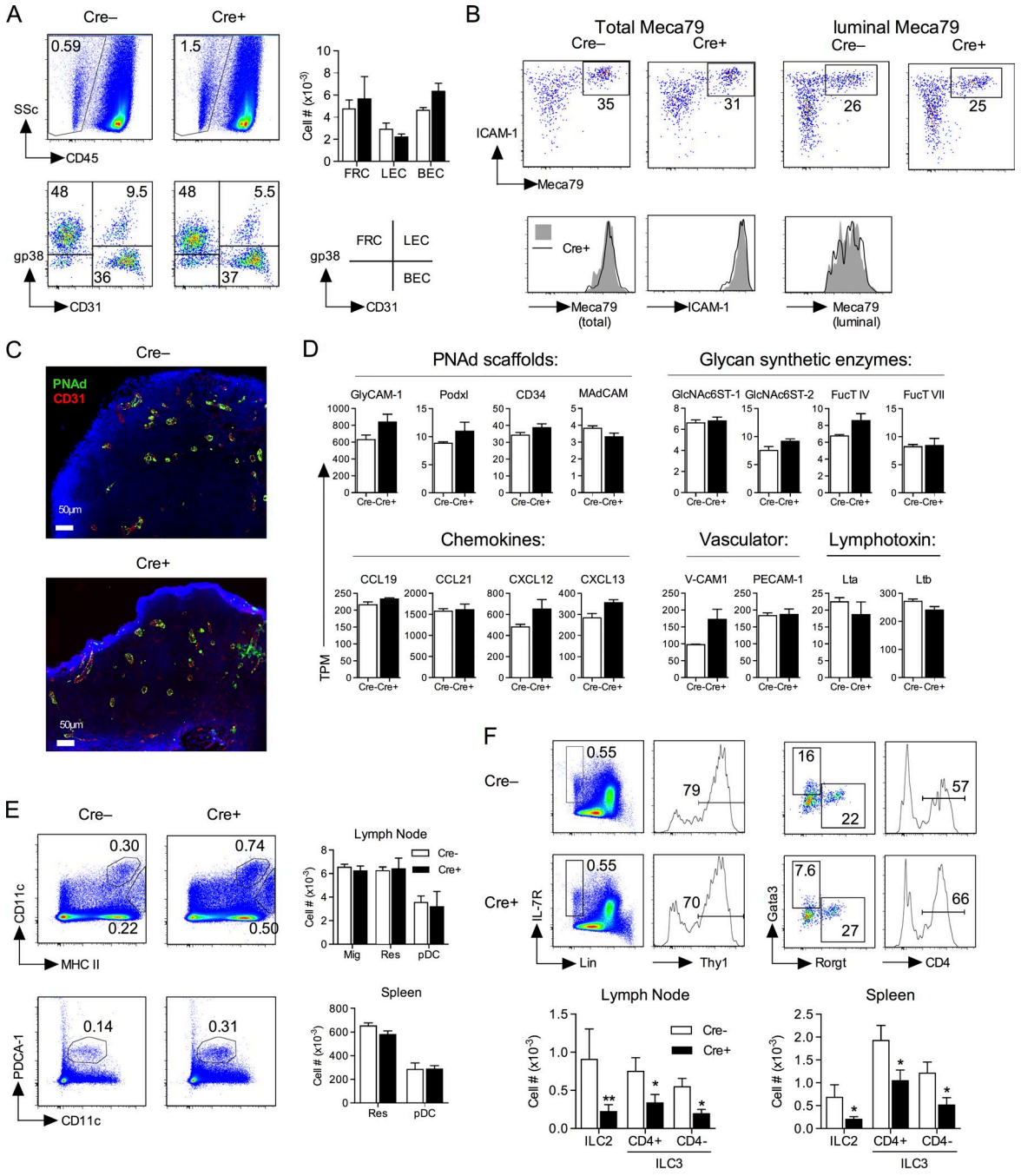

Figure 3. **Normal numbers of stromal and dendritic subsets but reduced ILC populations in lymph nodes after IL-7 ablation.** *Il7*$^{fx/KO}$ *R26*^{CreERT2} mice ($n = 4$) and CreERT –ve littermate controls ($n = 4$) were treated with tamoxifen for 5 d. 3 wk later, lymph nodes were recovered and cell composition analyzed by FACS. **(A)** Density plots are of CD45 vs. SSc on total live cells and show CD45$^-$ gate used to display gp38 vs CD31 (PECAM-1) density plots used to identify FRCs, LECs, and BECs. Bar chart shows total numbers of these subsets recovered from *R26*^{CreERT2} +ve (closed bars) and *R26*^{CreERT2} –ve *Il7*$^{fx/KO}$ mice (open bars). **(B)** Density plots are of Meca79 vs. anti-ICAM-1 staining by CD31$^+$gp38$^-$ BECs from representative mice described in A. Meca79 was either stained ex vivo in cell suspensions (Total Meca79) or by injection of mice with Meca79 mAb before ex vivo staining and analysis (luminal Meca79). Histograms are of ICAM-1 and Meca79 staining (total vs. luminal) by cells from Cre+ (solid line) or Cre– litter mates (gray shading), gated on Meca79$^+$ICAM-1$^+$ cells defined by the gate shown on density plots. **(C)** Frozen sections from lymph nodes from the indicated mice were analyzed for expression of PNAd (green), CD31 (red), and counterstained with nuclear DAPI staining. **(D)** *Il7*$^{fx/KO}$ *R26*^{CreERT2} mice ($n = 3$) and CreERT –ve littermate controls ($n = 3$) were treated with tamoxifen for 5 d. 3 wk later, total mRNA was isolated from total lymph nodes of individual mice and gene expression determined by RNAseq. Bar charts show mRNA expression level in transcripts per kilobase million (TPM) of the indicated genes. **(E)** Density plots are of CD11c vs. Class II MHC (MHC II) and PDCA-1 vs. CD11c, used to identify MHC II$^+$CD11c^{Hi} resident DC (Res), MHC II^{Hi} CD11c$^+$ migratory DC (Mig), and PDCA-1$^+$CD11c$^+$ plasmacytoid DCs (pDC). Bar charts show total numbers of these DC subsets recovered from the lymph nodes and spleen of *R26*^{CreERT2} +ve and *R26*^{CreERT2} –ve *Il7*$^{fx/KO}$ mice. **(F)** Density plots are of IL-7R vs. Lin; histograms are of Thy1 expression by IL-7R$^+$lin$^-$-gated cells. Density plots are of Gata3 vs. RORgt expression by Thy1$^+$ IL-7R$^+$lin$^-$ ILCs. Histograms are of CD4 expression by RORgt+ ILCs. Bar charts show total numbers of ILC subsets isolated from the lymph nodes and spleen of *R26*^{CreERT2} +ve and *R26*^{CreERT2} –ve *Il7*$^{fx/KO}$ mice. Data are representative of three independent experiments (A–D), a pool of two experiments (E), or four independent experiments (F). *, $P < 0.05$; **, $P < 0.01$. Error bars show SEM.

entry of lymphocytes into lymph nodes of treated hosts in short-term homing assays. Significantly, migration of both T and B cells into lymph nodes was reduced in anti–IL-7R–treated hosts (Fig. 4 C) but not migration into the spleen (Fig. 4 D). Analyzing lymph nodes of treated *Zap70*$^{-/-}$ and *Rag1*$^{-/-}$ mice revealed that ILC numbers were in both cases substantially reduced after blockade of IL-7R (Fig. 4 E). Therefore, the requirement for IL-7 for normal lymphocyte migration into lymph nodes did not depend on the prior presence of T or B lymphocytes within lymph nodes and correlated with the presence of ILC populations. Because IL-7Rα chain is also a component of the TSLP receptor, A7R34 could also act by blocking TSLP signaling. Although lymphoid development is normal in *Tslp*$^{-/-}$ mice (Al-Shami et al., 2004), we do not exclude a nonredundant role for TSLP alongside IL-7 in the lymphocyte homing phenotype.

ILC3s are required for normal migration of lymphocytes into lymph nodes

Our data reveal that IL-7 was constitutively required for normal migration of lymphocytes into lymph nodes and was independent of the presence of T or B cells within nodes. Stromal and DC populations were seemingly unaffected by loss of IL-7. Our analysis did reveal a specific loss of ILCs within lymph nodes. Specific ablation of ILC2s has no impact on lymph node size or composition (Oliphant et al., 2014). We therefore hypothesized that ILC3s may be required for normal entry of lymphocytes into nodes and that the role of IL-7 in this function was to ensure homeostatic maintenance of these ILC populations within lymph nodes. To test this, we analyzed lymphocyte entry into lymph nodes of experimental mice specifically deficient in ILC3s. *Rorc*$^{-/-}$ mice lack ILC3 populations but consequently lack lymph node structures because of the developmental requirements for ILC3s. Therefore, we generated bone marrow chimeras in which lethally irradiated WT hosts were reconstituted with bone marrow from *Rorc*$^{-/-}$ donors and conditioned with anti-Thy1 mAb to help eliminate radioresistant ILCs. In these chimeras, donor bone marrow failed to reconstitute ILC3 populations, and the combination of irradiation and anti-Thy1 treatment resulted in a substantial reduction in host ILC3 populations (Fig. 5 A). Initial analysis of chimeras revealed a reduction in the total size of the lymph node compartment of WT chimeras reconstituted with donor *Rorc*$^{-/-}$ bone marrow (Fig. 5 B). Testing the ability of lymphocytes to enter lymph nodes revealed that entry of both T and B lymphocytes (Fig. 5 C) was profoundly impaired in chimeras reconstituted with *Rorc*$^{-/-}$ bone marrow. Histological analysis of lymph nodes from chimeras revealed grossly normal CD31^{+} HEV structures in which PNAd expression was readily detectable (Fig. 5 D). Finally, we asked whether homing defects induced after IL-7R blockade could be specifically rescued by ILC3s. To do this, we generated control and *Rorc*$^{-/-}$ chimeras using CD45.1 hosts that were conditioned with anti–IL-7R treatment at the time of reconstitution. Blocking IL-7R in chimeras resulted in the expected defect in lymphocyte homing to lymph nodes by 2 wk after bone marrow transplant (BMT), compared with chimeras treated with isotype control mAb (Fig. 5 E). Analyzing ILC subsets in fully reconstituted chimeras revealed that anti–IL-7R–treated hosts given WT bone marrow were able to partially reconstitute ILC3s in lymph

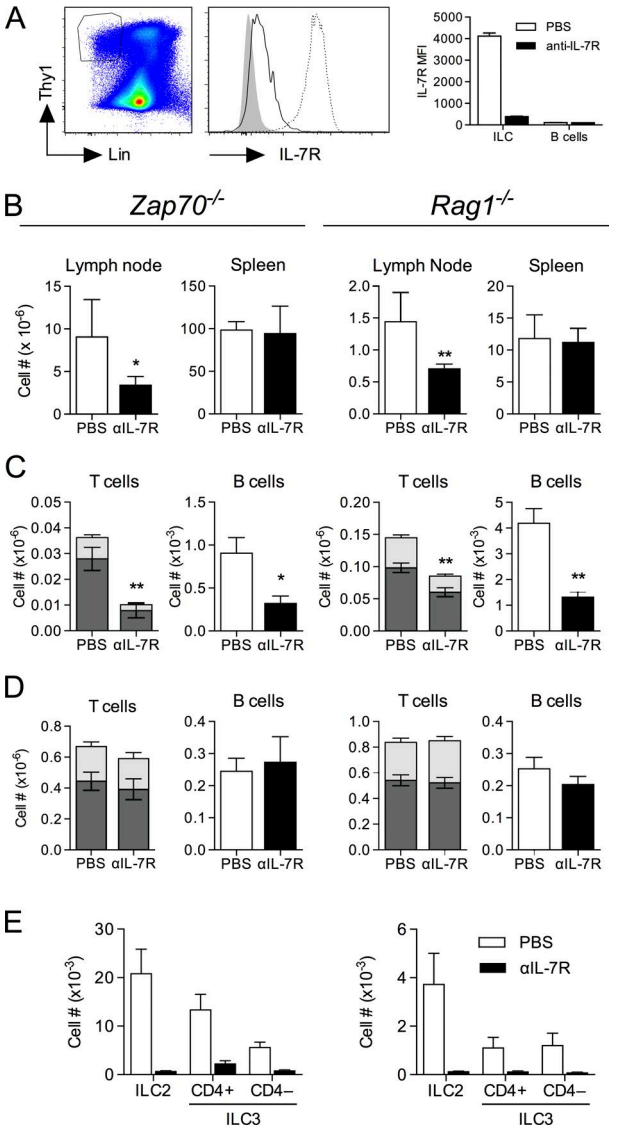

Figure 4. **IL-7 blockade in vivo impairs lymphocyte entry into lymph nodes but not spleen.** Cohorts of *Zap70*$^{-/-}$ and *Rag1*$^{-/-}$ hosts were i.p. injected three times per week for 2 wk with either A7R34 anti-IL-7R mAb or PBS as control. Hosts were then injected i.v. with 10^7 total lymph node cells from CD45.1 congenic donors. 1 h later, host the lymph nodes and spleen were analyzed by FACS. **(A)** Density plot is of Thy1 vs. Lin to indicate ILC gate. Histogram is of IL-7R expression by ILCs in PBS-treated (broken line) vs. A7R34-treated *Zap70*$^{-/-}$ hosts (solid line), compared with B cells in PBS-treated hosts (gray shading). Bar chart shows MFI of IL-7R by ILC and B cells in the indicated hosts. **(B)** Bar charts are of total cell numbers recovered from the lymph nodes or spleen of the indicated hosts treated with either anti-IL-7R mAb (αIL-7R, shaded bars) or PBS as control (white bars). **(C and D)** Stacked bar charts indicate the combined total of donor CD4 (dark gray) and CD8 (light gray) T cells recovered from the lymph nodes (C) or spleen (D) of *Zap70*$^{-/-}$ (left column) or *Rag1*$^{-/-}$ hosts (right column). Bar charts are of donor B cells recovered from the same hosts. **(E)** Bar charts show total host ILC subsets recovered from the lymph nodes of the indicated hosts treated with either anti-IL-7R mAb (αIL-7R, shaded bars) or PBS as control (white bars). Data are the pool of three (*Zap70*$^{-/-}$ hosts, $n = 8$ per group; *Rag1*$^{-/-}$ hosts, $n = 11$ per group) independent experiments. In one replicate experiment, *Zap70*$^{-/-}$ hosts receiving 2A3 isotype control vs. A7R34 generated equivalent data to those using PBS control for A7R34. *, $P < 0.05$; **, $P < 0.01$. Error bars show SEM.

nodes when compared with isotype control-treated chimeras, although recipients of *Rorc*$^{-/-}$ bone marrow reconstituted only ILC2 populations (Fig. 5, F and G). Importantly, assaying short-term lymphocyte homing to lymph nodes in the different hosts revealed that lymphocyte homing was also partially rescued in anti–IL-7R–treated WT chimeras, compared with isotype-treated controls, and anti–IL-7R–treated *Rorc*$^{-/-}$ chimeras in which lymphocyte homing remained impaired (Fig. 5 H).

The role of IL-7 in the development of lymph node structures in neonates has long been recognized. Our new data reveal that IL-7 continues to play an important role in the normal function of lymph nodes in adulthood too, because ablation of IL-7 expression or activity resulted in impaired migration of T and B cells into lymph nodes. In neonates, IL-7 is required for development of LTi/ILC3s, and it appears that their maintenance in adults continues to be IL-7 dependent, and the persistence of ILC3s remains important for normal lymph node function. We did not find any obvious defects in the positive regulators of HEV function after IL-7 ablation. The key structures and cues required for the migration of T and B cells into lymph nodes appeared intact. However, there is also evidence that HEVs are maintained in a dynamic equilibrium that balances cellular exclusion and permeability to cells in the blood (Herzog et al., 2013), raising the possibility that ILC3s may counter forces of exclusion, rather than positively regulate mechanisms of entry. Identifying these mechanisms will be important subjects for future studies.

Our data also reveal another important function for IL-7 production by stroma in promoting optimal immunity. There is good evidence that loss of IL-7 production by stroma underlies thymic atrophy suffered during aging. It seems likely that stromal components of other lymphoid tissues may suffer a similar loss of IL-7–producing capacity with age. Therefore, the effects on lymphocyte recirculation through lymph nodes in the absence of optimal IL-7 production may represent an additional consequence of aging, in addition to the anticipated effects on T cell development and maintenance, that together contribute to loss of immunity in old age. Our findings therefore identify an additional potential mechanism by which IL-7 therapy may help restore immune function as a consequence of age-related loss of endogenous cytokine.

Materials and methods

Mice

ES cells bearing the *Il7*$^{tm1a(EUCOMM)Wtsi}$ targeted mutation were purchased from the European Mouse Mutant Cell Repository and used to generate chimeric mice by standard blastocyst injection. Null (*Il7*^{LacZKO}) and conditional (*Il7*^{flox}) alleles of the *Il7* gene were generated by intercrossing *Il7*$^{tm1a(EUCOMM)Wtsi}$ mice with PC3-Cre and actin-FlpE strains, respectively (Fig. S1 A). All mouse strains used in this study were bred in a conventional colony free of pathogens at the National Institute for Medical Research in London and the Comparative Biology Unit, University College London (UCL). Two experiments using *Rorc*$^{-/-}$ chimeras and controls were performed in the Department of Hematology, Erasmus University Medical Center, Rotterdam, Netherlands. All mice were on a C57BL/6J background (N5). 5 mg tamoxifen (T5648; Sigma) dissolved in corn oil (C8267; Sigma) was given daily to mice by oral gavage for 5 consecutive days. Groups of mice were treated with anti–IL-7R mAb (Clone A7R34; Bio X Cell), 0.3 mg/injection delivered i.p. three times per week. Controls received injections of PBS or isotype (Clone 2A3; Bio X Cell). Chimeras were generated by irradiating WT hosts with 9 Gy. WT hosts were then injected with 1–1.5 × 10^7 bone marrow cells from *Rorc*$^{-/-}$ or WT control donors. To eliminate residual radioresistant host ILC3s, 2 wk after bone marrow reconstitution, chimeras received five i.p. injections of 200 µg α-Thy1 antibody over 2 wk (YTS154; provided by H. Waldmann; Aparicio-Domingo et al., 2015). Animal experiments were performed according to the UCL Animal Welfare and Ethical Review Body and Home Office regulations.

Flow cytometry

Normally, thymus, spleen, and mesenteric and peripheral lymph nodes were meshed through a 70-µm nylon mesh, and the cell concentrations were determined with a Scharf Instruments Casy Counter. Inguinal, cervical, axillary, and brachial lymph nodes were dissected in individual mice. For the isolation of ILCs and DCs, individual lymph nodes were pierced with fine forceps and digested for 25 min at 37°C in RPMI with 0.42 mg/ml Liberase TL (Roche) and 0.1 mg/ml DNase I (Roche). The reaction was stopped with 10 mM EDTA. Digested tissue was then crushed through a 70-µm nylon mesh. Stromal cells were isolated as previously described (Fletcher et al., 2011). For the detection of luminal PNAd, mice were injected i.v. with 50 µg biotin-conjugated MECA-79 (clone Meca79; Biolegend) and sacrificed after 20 min. Cells were incubated with saturating concentrations of antibodies in 100 µl PBS containing BSA (0.1%) and 1 mM azide (PBS-BSA-azide) for 45 min at 4°C followed by two washes in PBS-BSA-azide. Antibodies raised against the following mouse antigens were used: CD3e (clone 145-2C11; eBioscience), CD4 (clone RM4-5; eBioscience, Biolegend), CD5 (clone 53-7.3; Biolegend), CD8 (clone 53-6.7; Biolegend, BD), CD19 (clone 6D5; Biolegend), CD24 (clone M1/69; Biolegend), CD25 (clone PC61.5; eBioscience, Biolegend), CD31 (clone 390; eBioscience, Biolegend), CD44 (clone IM7; eBioscience, BD), CD45.1 (clone A20; Biolegend), CD45.2 (Clone 104; eBioscience, Biolegend), CD122 (clone 5H4; eBioscience), TCRβ (clone H57-597;eBioscience, Biolegend), TCRγδ (clone GL3; Biolegend), B220 (clone RA3-6B2; Biolegend), CD11b (clone M1/70; Biolegend), CD11c (clone N418; Biolegend), PDCA-1 (clone 129c1; Biolegend), MHCII (clone M5/114.15.2; eBioscience), gp38 (clone eBio8.1.1; eBioscience), Meca79 (clone Meca79; Biolegend), ICAM-1 (clone YN1/1.7.4; Biolegend), Thy1.2 (clone 30-H12; Biolegend), IL-7Rα (clone A7R34; eBioscience), F4/80 (cloneBM8; Biolegend), CD49b (clone DX5; Biolegend), GR1 (clone RB6-8C5; Biolegend), Ter-119 (clone Ter-119; Biolegend), NK1.1 (clone PK136; Biolegend), GATA3 (clone L50-823; BD), RORγT (clone Q31-378; BD), and Streptavidin BUV737 (BD). In the thymus, the lineage dump channel for CD4 CD8 double-negative populations contained antibodies against GL3, CD19, GR1, CD11b, F4/80, NK1.1, and CD11c. In lymph nodes, the lineage stain for ILCs contained antibodies against CD3e, TCRβ, GL3, CD19, GR1, CD11b, and F4/80 except in Figs. 4 and 5 where additional Ter-119, NK1.1, CD49b, and CD11c were included. Cell viability was determined by using the LIVE/

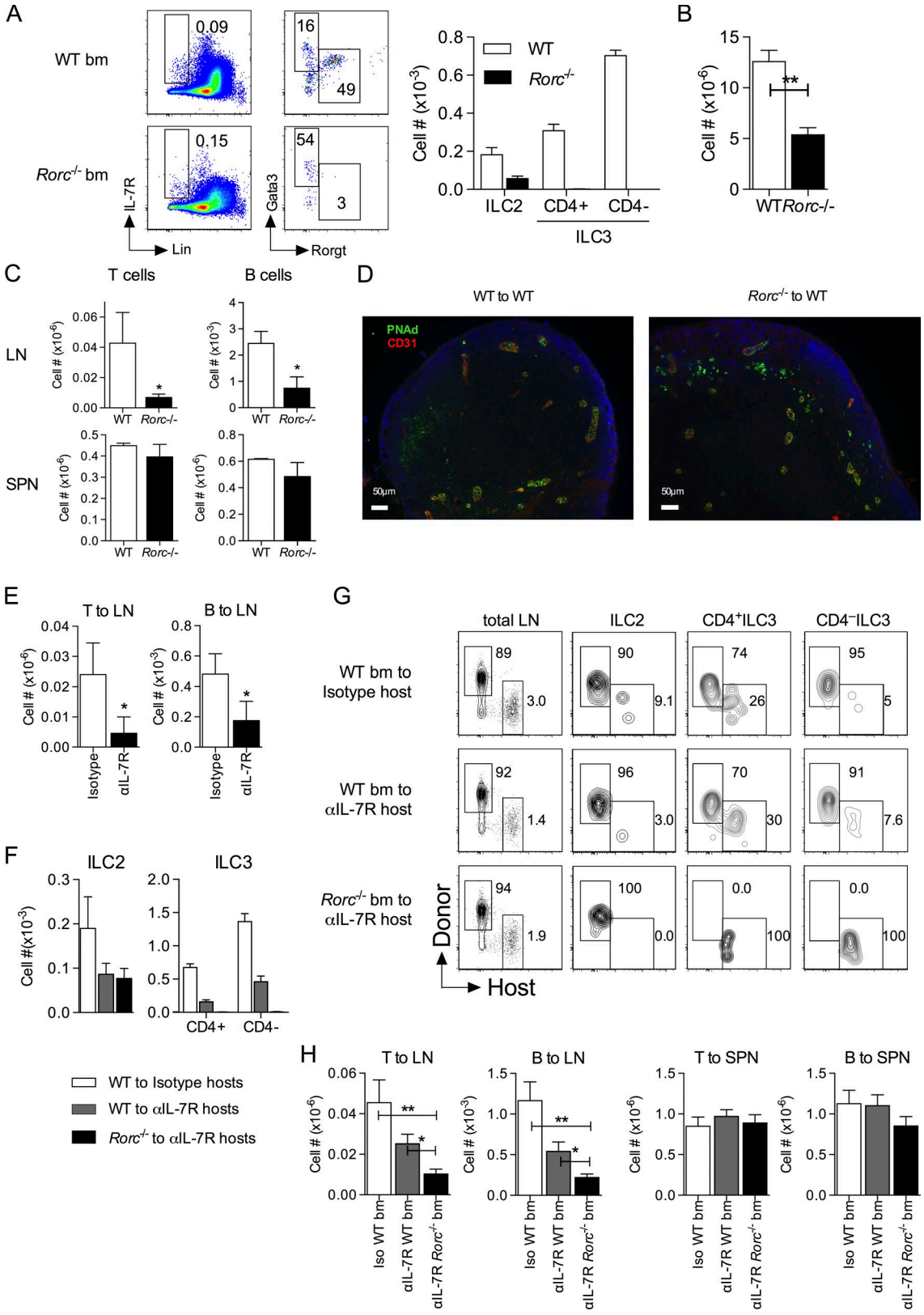

Figure 5. **Lymphocyte entry into lymph nodes is defective in the absence of ILC3s. (A–D)** Mice specifically lacking ILC3s were generated by reconstitution of irradiated WT hosts with bone marrow from *Rorc*$^{-/-}$ (n = 9) or WT (n = 10) donor bone marrow as control. Both groups were also treated with anti-Thy1 for 2 wk after BMT. 12 wk after reconstitution, hosts were injected with 10^7 labeled WT lymphocytes from either the spleen or a mixture of the lymph nodes and spleen, and 1 or 3 h later cell numbers in the lymph nodes and spleen were determined by FACS. **(A)** Density plots are of IL-7R vs. Lin for total lymphocytes and Gata3 vs. RORgt by IL-7R$^+$Lin$^-$-gated cells. Bar charts show total numbers of ILC subpopulations in the indicated chimeras. **(B)** Bar charts are of total lymph

DEAD cell stain kit (Invitrogen Molecular Probes). Intracellular staining was performed by using the FoxP3 fixation and permeabilization kit (eBioscience). The addition of SPHEROTM AccuCount fluorescent particles (Spherotech, Inc.) was used to calculate cell frequencies. 8–13-color flow cytometric staining was analyzed on a FACSCanto II or LSRFortessa X-20 (Becton Dickinson) instrument, and data analysis and color compensations were performed with FlowJo V9.5.3 software (TreeStar). Data are displayed on log and biexponential displays.

Short-term migration assay

10^7 lymphocytes from lymph nodes, and in indicated experiments also the spleen, were injected i.v. into groups of experimental mice. 1 h later, lymph node, spleen, and blood samples were recovered and analyzed by FACS. Numbers of donor cells present in different organs were determined on the basis of either prior CTV labeling (0.5 µM; Thermo Fisher Scientific) or expression of congenic CD45.1 by adding counting beads to samples and analyzing cells by flow cytometry.

RNA sequencing and real-time quantitative PCR

Tissue samples were homogenized in 600 µl RLT lysis buffer (Qiagen) by using a Precellys Homogenizer, and RNA was isolated by using the RNeasy Mini kit (Qiagen) according to the manufacturer's instructions. RNA integrity was confirmed by using Agilent's 2100 Bioanalyzer. mRNA libraries were prepared by using the KAPA mRNA Hyper Prep kit (Roche), following manufacturer's instructions. 75-bp single-end reads were generated by using an Illumina HiSeq 2500. The raw Illumina reads were analyzed as follows: Read trimming and adapter removal were performed by using Trimmomatic (version 0.36). The RSEM package (version 1.2.31) together with STAR (version 2.5.2a) were used to align reads to the mouse genome (ensembl GRCm38 release 86) and to obtain gene level counts. Differential expression analysis was performed by using DESeq2 package (version 1.14.1) within R version 3.3.2. Data are deposited in ArrayExpress, accession no. E-MTAB-6451. For real-time PCR, cDNA was produced by reverse transcription, and levels of *Il7* mRNA (FAM probeMm01295803_m1; AppliedBiosystems) were determined using Applied Biosystems ABI Prism 7900 sequence detection system. *Il7* mRNA levels were normalized against *Hprt1* mRNA (FAM probe Mm00446968_m1).

Immunohistochemistry

6-µm cryosections were fixed for 5 min in ice-cold acetone and air-dried for an additional 10 min. After blocking of Fc receptors with serum, sections were incubated with primary antibodies for 1 h at room temperature, followed by a 30-min incubation with a Fluor-Alexa-labeled conjugate (Molecular Probes). Sections were embedded in ProLong Gold (Invitrogen) and analyzed on a Leica DMRXA fluorescent microscope. The antibodies used were CD31 (clone 390; eBioscience), PNAd (Meca79; supernatant was provided by R. Mebius, VU University Medical Center Amsterdam, Amsterdam, Netherlands).

Statistics

Statistical analysis and figure preparation were performed by using Graphpad Prism 6 (v6.0a). Column data were compared by nonparametric unpaired two-tailed Mann–Whitney test. *, $P < 0.05$; **, $P < 0.01$.

Online supplemental material

Fig. S1 shows the phenotype of $Il7^{LacZKO}$ mice.

Acknowledgments

We thank Louise Webb for technical assistance, the former Medical Research Council National Institute for Medical Research (NIMR) Biological Services, and UCL Comparative Biology Unit staff for assistance with mouse breeding, and The Francis Crick Institute Advanced Sequencing Facility and Bioinformatics and Biostatistics Facility for assistance with performing RNA-seq analysis. We thank Ann Ager for advice and discussion and David Withers for kindly providing bone marrow from *Rorc*$^{-/-}$ donors and discussion.

This work was supported by the Medical Research Council under program codes MC_PC_13055 and MR/P011225/1, project award G0601156, by ZonMW Innovative Research Incentives Vidi grant 91710377 (to T. Cupedo) and Veni grant 91615128 (to F. Cornelissen).

The authors declare no competing financial interests.

Author contributions: J. Yang designed and performed the experiments and reviewed and edited the manuscript. F. Cornelissen designed and performed the experiments. N. Papazian performed the experiments. R.M. Reijmers designed and performed the experiments. M. Llorian performed the experiments. T. Cupedo designed the experiments and reviewed and edited

node size in chimeras of WT hosts reconstituted with either *Rorc*$^{-/-}$ or WT bone marrow. **(C)** Bar charts show the recovery of donor T and B cells from the indicated *Rorc*$^{-/-}$ chimeras from either lymph nodes (LN) or spleen (SPN). **(D)** Frozen sections from lymph nodes from the indicated chimeras were analyzed for expression of PNAd (green), CD31 (red) and counterstained with nuclear DAPI staining. **(E–H)** CD45.1 hosts were irradiated and reconstituted with either WT or *Rorc*$^{-/-}$ bone marrow. WT chimeras were treated with either anti-IL-7R or isotype control for 1 wk after irradiation, whereas *Rorc*$^{-/-}$ chimeras all received anti-IL-7R mAb. **(E)** 2 wk after BMT, groups of anti-IL-7R (αIL-7R) and isotype-treated WT chimeras ($n = 3$ per group) were injected with labeled lymphocytes. Bar charts show numbers of T and B cells in lymph nodes 1 h after transfer. **(F)** 12 wk after BMT, lymph nodes were analyzed by FACs. Bar chart shows total numbers of ILC populations in lymph nodes from isotype-treated WT chimeras (white bars), anti-IL-7R (αIL-7R)-treated WT chimeras (gray bars), and anti-IL-7R (αIL-7R)-treated *Rorc*$^{-/-}$ chimeras (black bars). **(G)** Density plots show CD45.1 host vs. CD45.2 donor cells among total lymphocytes, gated ILC2, CD4$^+$ILC3, and CD4$^-$ ILC3 in the indicated chimeras. **(H)** 12 wk after BMT, chimeras ($n = 7$ per group) were injected with labeled WT cells from mixture of the lymph nodes and spleen, and 1 h later the host lymph nodes and spleen were analyzed by FACS. Bar charts show the numbers of donor T and B cells recovered from the lymph nodes and spleen of the indicated chimeras. Data are pools of four (B and C) or two (A, D, and E–H) independent experiments. E, F, and H are also representative of one further experiment performed by using WT CD45.2 hosts. *, $P < 0.05$; **, $P < 0.01$. Error bars show SEM.

manuscript. M. Coles designed the experiments and reviewed and edited the manuscript. B. Seddon designed the experiments and wrote, reviewed and edited the manuscript.

Submitted: 21 March 2017
Revised: 21 December 2017
Accepted: 29 January 2018

References

Acton, S.E., A.J. Farrugia, J.L. Astarita, D. Mourão-Sá, R.P. Jenkins, E. Nye, S. Hooper, J. van Blijswijk, N.C. Rogers, K.J. Snelgrove, et al. 2014. Dendritic cells control fibroblastic reticular network tension and lymph node expansion. *Nature.* 514:498–502. https://doi.org/10.1038/nature13814

Al-Shami, A., R. Spolski, J. Kelly, T. Fry, P.L. Schwartzberg, A. Pandey, C.L. Mackall, and W.J. Leonard. 2004. A role for thymic stromal lymphopoietin in CD4(+) T cell development. *J. Exp. Med.* 200:159–168. https://doi.org/10.1084/jem.20031975

Aparicio-Domingo, P., M. Romera-Hernandez, J.J. Karrich, F. Cornelissen, N. Papazian, D.J. Lindenbergh-Kortleve, J.A. Butler, L. Boon, M.C. Coles, J.N. Samsom, and T. Cupedo. 2015. Type 3 innate lymphoid cells maintain intestinal epithelial stem cells after tissue damage. *J. Exp. Med.* 212:1783–1791. https://doi.org/10.1084/jem.20150318

Browning, J.L., N. Allaire, A. Ngam-Ek, E. Notidis, J. Hunt, S. Perrin, and R.A. Fava. 2005. Lymphotoxin-beta receptor signaling is required for the homeostatic control of HEV differentiation and function. *Immunity.* 23:539–550. https://doi.org/10.1016/j.immuni.2005.10.002

Buentke, E., A. Mathiot, M. Tolaini, J. Di Santo, R. Zamoyska, and B. Seddon. 2006. Do CD8 effector cells need IL-7R expression to become resting memory cells? *Blood.* 108:1949–1956. https://doi.org/10.1182/blood-2006-04-016857

Coles, M.C., H. Veiga-Fernandes, K.E. Foster, T. Norton, S.N. Pagakis, B. Seddon, and D. Kioussis. 2006. Role of T and NK cells and IL7/IL7r interactions during neonatal maturation of lymph nodes. *Proc. Natl. Acad. Sci. USA.* 103:13457–13462. https://doi.org/10.1073/pnas.0604183103

Cupedo, T., M.F. Vondenhoff, E.J. Heeregrave, A.E. De Weerd, W. Jansen, D.G. Jackson, G. Kraal, and R.E. Mebius. 2004. Presumptive lymph node organizers are differentially represented in developing mesenteric and peripheral nodes. *J. Immunol.* 173:2968–2975. https://doi.org/10.4049/jimmunol.173.5.2968

Eberl, G., S. Marmon, M.J. Sunshine, P.D. Rennert, Y. Choi, and D.R. Littman. 2004. An essential function for the nuclear receptor RORgamma(t) in the generation of fetal lymphoid tissue inducer cells. *Nat. Immunol.* 5:64–73. https://doi.org/10.1038/ni1022

Fletcher, A.L., D. Malhotra, S.E. Acton, V. Lukacs-Kornek, A. Bellemare-Pelletier, M. Curry, M. Armant, and S.J. Turley. 2011. Reproducible isolation of lymph node stromal cells reveals site-dependent differences in fibroblastic reticular cells. *Front. Immunol.* 2:35. https://doi.org/10.3389/fimmu.2011.00035

Herzog, B.H., J. Fu, S.J. Wilson, P.R. Hess, A. Sen, J.M. McDaniel, Y. Pan, M. Sheng, T. Yago, R. Silasi-Mansat, et al. 2013. Podoplanin maintains high endothelial venule integrity by interacting with platelet CLEC-2. *Nature.* 502:105–109. https://doi.org/10.1038/nature12501

Kim, G.Y., C. Hong, and J.H. Park. 2011. Seeing is believing: Illuminating the source of in vivo interleukin-7. *Immune Netw.* 11:1–10. https://doi.org/10.4110/in.2011.11.1.1

Link, A., T.K. Vogt, S. Favre, M.R. Britschgi, H. Acha-Orbea, B. Hinz, J.G. Cyster, and S.A. Luther. 2007. Fibroblastic reticular cells in lymph nodes regulate the homeostasis of naive T cells. *Nat. Immunol.* 8:1255–1265. https://doi.org/10.1038/ni1513

Moussion, C., and J.P. Girard. 2011. Dendritic cells control lymphocyte entry to lymph nodes through high endothelial venules. *Nature.* 479:542–546. https://doi.org/10.1038/nature10540

Oliphant, C.J., Y.Y. Hwang, J.A. Walker, M. Salimi, S.H. Wong, J.M. Brewer, A. Englezakis, J.L. Barlow, E. Hams, S.T. Scanlon, et al. 2014. MHCII-mediated dialog between group 2 innate lymphoid cells and CD4(+) T cells potentiates type 2 immunity and promotes parasitic helminth expulsion. *Immunity.* 41:283–295. https://doi.org/10.1016/j.immuni.2014.06.016

Onder, L., P. Narang, E. Scandella, Q. Chai, M. Iolyeva, K. Hoorweg, C. Halin, E. Richie, P. Kaye, J. Westermann, et al. 2012. IL-7-producing stromal cells are critical for lymph node remodeling. *Blood.* 120:4675–4683. https://doi.org/10.1182/blood-2012-03-416859

Onder, L., R. Danuser, E. Scandella, S. Firner, Q. Chai, T. Hehlgans, J.V. Stein, and B. Ludewig. 2013. Endothelial cell-specific lymphotoxin-β receptor signaling is critical for lymph node and high endothelial venule formation. *J. Exp. Med.* 210:465–473. https://doi.org/10.1084/jem.20121462

Satoh-Takayama, N., S. Lesjean-Pottier, P. Vieira, S. Sawa, G. Eberl, C.A. Vosshenrich, and J.P. Di Santo. 2010. IL-7 and IL-15 independently program the differentiation of intestinal CD3-NKp46+ cell subsets from Id2-dependent precursors. *J. Exp. Med.* 207:273–280. https://doi.org/10.1084/jem.20092029

Schluns, K.S., W.C. Kieper, S.C. Jameson, and L. Lefrançois. 2000. Interleukin-7 mediates the homeostasis of naïve and memory CD8 T cells in vivo. *Nat. Immunol.* 1:426–432. https://doi.org/10.1038/80868

Seddon, B., and R. Zamoyska. 2002. TCR signals mediated by Src family kinases are essential for the survival of naive T cells. *J. Immunol.* 169:2997–3005. https://doi.org/10.4049/jimmunol.169.6.2997

Sudo, T., S. Nishikawa, N. Ohno, N. Akiyama, M. Tamakoshi, H. Yoshida, and S. Nishikawa. 1993. Expression and function of the interleukin 7 receptor in murine lymphocytes. *Proc. Natl. Acad. Sci. USA.* 90:9125–9129. https://doi.org/10.1073/pnas.90.19.9125

Sun, Z., D. Unutmaz, Y.R. Zou, M.J. Sunshine, A. Pierani, S. Brenner-Morton, R.E. Mebius, and D.R. Littman. 2000. Requirement for RORgamma in thymocyte survival and lymphoid organ development. *Science.* 288:2369–2373. https://doi.org/10.1126/science.288.5475.2369

von Andrian, U.H., and T.R. Mempel. 2003. Homing and cellular traffic in lymph nodes. *Nat. Rev. Immunol.* 3:867–878. https://doi.org/10.1038/nri1222

von Freeden-Jeffry, U., P. Vieira, L.A. Lucian, T. McNeil, S.E. Burdach, and R. Murray. 1995. Lymphopenia in interleukin (IL)-7 gene-deleted mice identifies IL-7 as a nonredundant cytokine. *J. Exp. Med.* 181:1519–1526. https://doi.org/10.1084/jem.181.4.1519

Wendland, M., S. Willenzon, J. Kocks, A.C. Davalos-Misslitz, S.I. Hammerschmidt, K. Schumann, E. Kremmer, M. Sixt, A. Hoffmeyer, O. Pabst, and R. Förster. 2011. Lymph node T cell homeostasis relies on steady state homing of dendritic cells. *Immunity.* 35:945–957. https://doi.org/10.1016/j.immuni.2011.10.017

Ye, S.K., Y. Agata, H.C. Lee, H. Kurooka, T. Kitamura, A. Shimizu, T. Honjo, and K. Ikuta. 2001. The IL-7 receptor controls the accessibility of the TCRgamma locus by Stat5 and histone acetylation. *Immunity.* 15:813–823. https://doi.org/10.1016/S1074-7613(01)00230-8